Journal of Alloys and Compounds 791 (2019) 947–951

Contents lists available at ScienceDirect

Journal of Alloys and Compounds

journal homepage: http://www.elsevier.com/locate/jalcom

New ferromagnetic $(Fe_{1/3}Co_{1/3}Ni_{1/3})_{80}(P_{1/2}B_{1/2})_{20}$ high entropy bulk metallic glass with superior magnetic and mechanical properties

Chunze Li [a], Qiang Li [a, *], Mingcan Li [a], Chuntao Chang [b, **], Hongxiang Li [c], Yaqiang Dong [d], Yanfei Sun [a]

[a] School of Physics Science and Technology, Xinjiang University, Urumqi, Xinjiang 830046, People's Republic of China
[b] School of Mechanical Engineering, Dongguan University of Technology, Dongguan, 523808, People's Republic of China
[c] State Key Laboratory for Advanced Metals and Materials, University of Science and Technology Beijing, Beijing 100083, People's Republic of China
[d] Zhejiang Province Key Laboratory of Magnetic Materials and Application Technology, Key Laboratory of Magnetic Materials and Devices, Ningbo Institute of Materials Technology &Engineering, Chinese Academy of Sciences, Ningbo, Zhejiang 315201, People's Republic of China

ARTICLE INFO

Article history:
Received 11 December 2018
Received in revised form
21 March 2019
Accepted 27 March 2019
Available online 30 March 2019

Keywords:
High entropy alloys
Bulk metallic glasses
Glass forming ability
Magnetic properties
Mechanical properties

ABSTRACT

New ferromagnetic $(Fe_{1/3}Co_{1/3}Ni_{1/3})_{80}(P_{1/2}B_{1/2})_{20}$ high entropy bulk metallic glass (HE-BMG) with the maximum diameter of 2 mm has been prepared by combining fluxing treatment and J-quenching technique. The present HE-BMG exhibits excellent soft magnetic properties with a saturation magnetization of 0.90 T, low coercivity of 1.5 A/m, high permeability of 10172 @ 1 kHz and low hysteresis loss of 21 kJ/mol @ 50 Hz (for the annealed glassy ribbon), and mechanical properties with a compressive yield strength of 3000 MPa and large plastic strain of 4%. The combination of superior glass-forming ability, excellent magnetic and mechanical properties makes the present HE-BMG a future promising application as advanced structural and functional materials.

1. Introduction

Due to the absence of dislocations, grain boundaries, crystallographic planes, etc., bulk metallic glasses (BMGs) exhibit excellent properties such as high strength near the theoretical prediction, large elastic strain, excellent magnetic properties, good corrosion and wear resistances compared with their crystalline counterparts [1,2]. High entropy alloys (HEAs), typically defined as the alloys composing of at least five principal elements in equal or near equal atomic percent (at.%) ranging from 5 to 35 at.% [3,4]. High mixing entropy of HEAs drives them to form simple solid solutions in face-centered-cubic (FCC), body-centered-cubic (BCC), or hexagonal close-packed (HCP) structure rather than complex microstructures with many compounds [3,5,6]. Due to the effects of solid solution strengthening, slow diffusion and high mixing entropy, HEAs exhibit many superior properties, such as high strength, high hardness, high wear resistance, good corrosion resistance and high temperature oxidation resistance, compared with common alloys [6–8]. Because of their considerably different characteristics in structure and composition design rules, the HEAs and BMGs have been studied independently until the HEAs with amorphous structure, named high entropy bulk metallic glasses (HE-BMGs), were successfully synthesized by Ma et al., in 2002 [9]. The appearance of HE-BMGs provides a new strategy to design advanced materials, which have excellent mechanical and physical properties inherited from the advantages of both HEAs and BMGs [10,11].

Until now, a series of HE-BMGs that exhibit unique physical and mechanical properties have been developed, e.g., Ti-Zr-Cu based HE-BMGs, rare earth-based HE-BMGs noble metals based HE-BMGs and magnetic transition metal based HE-BMGs [10,12–14]. Due to the low raw material cost and potential application as magnetic materials, a number of researchers have paid much attention to the magnetic transition metal based HE-BMGs For instance, Li et al. successfully developed $Fe_{25}Co_{25}Ni_{25}(P_{0.3}C_{0.3}B_{0.4})_{25}$ HE-BMGs that has a yield strength of 3210 MPa [15]. Subsequently, the $Fe_{25}Co_{25}Ni_{25}(B_{0.7}Si_{0.3})_{25}$ HE-BMGs, which has a yield strength of 3624 MPa was synthesized by Qi et al. [16]. However, most of recently developed magnetic transition metal based HE-BMGs exhibit a

* Corresponding author.
** Corresponding author.
E-mail addresses: qli@xju.edu.cn (Q. Li), ctchang@nimte.ac.cn (C. Chang).

https://doi.org/10.1016/j.jallcom.2019.03.375
0925-8388/

poor room temperature plasticity. In addition, the saturation magnetization is always lower than 0.9 T, which can be attributed to the relatively low magnetic elements content (usually less than 75 at.%). Therefore, developing the new ferromagnetic magnetic transition metal based HE-BMGs with both excellent magnetic properties and superior mechanical properties has been earnestly desired from academia to industry.

For the metal-metalloid type, the best composition to form a glass is around 80 at.% of the metal component and 20 at.% of the metalloid component [17]. According to this composition and the compositional design rule of high entropy alloys, we successfully developed a new ferromagnetic $(Fe_{1/3}Co_{1/3}Ni_{1/3})_{80}(P_{1/2}B_{1/2})_{20}$ HE-BMG with a critical diameter of 2 mm by combining fluxing purification treatment and J-quenching technique in this work. At the same time, the thermal stability, magnetic and mechanical properties of the new ferromagnetic HE-BMG have been systematically investigated.

2. Experimental procedure

The mother alloy ingots of $(Fe_{1/3}Co_{1/3}Ni_{1/3})_{80}(P_{1/2}B_{1/2})_{20}$ were prepared by torch-melting a mixture of pure Fe powders (99 mass %), Co powders (99.9 mass%), Ni powders (99.7 mass%),Co_2P powders (98 mass%), and B pieces (99.95 mass%) under a high-purity argon atmosphere. Subsequently, the mother alloy ingots were fluxed in a fluxing agent composed of B_2O_3 and CaO with a mass ratio of 3:1 at an elevated temperature of 1500 K for about 4 h under a vacuum of ~50 Pa. After fluxed treatment, the alloy ingots were cooled down to room temperature and then subjected to the J-quenching technique. As a result, cylindrical alloy samples with a diameter of 1–2 mm and a length of a few centimeters were prepared. The details about J-quenching technique can be found elsewhere [18]. Additionally, in order to measure the coercivity, amorphous ribbons of $(Fe_{1/3}Co_{1/3}Ni_{1/3})_{80}(P_{1/2}B_{1/2})_{20}$ with a width of about 1 mm and a thickness of 40 μm were prepared by injecting the remelted ingots onto a spinning copper wheel.

The glassy nature of the samples was identified by X-ray diffraction (XRD, Bruker D8 Advance) using a Cu-K_α radiation at a scan rate of 6°/min. The morphology of the samples was observed by a high resolution transmission electron microscopy (HRTEM, JEOL JEM-2010F). The thermal behavior of the samples was examined by differential scanning calorimetry (DSC, NETZSCH DSC 404F1) at a heating rate of 0.33 K/s under an Ar atmosphere. The saturation magnetization was measured for the bulk samples by vibrating sample magnetometer (VSM, Lake Shore 7410) with a maximum applied field of 800 kA/m at room temperature. The density of the samples was determined by the Archimedes drainage method using distilled water as working liquid. The magnetic properties including coercivity, permeability and hysteresis loss were measured for as-quenched/annealed glassy ribbon samples with the same composition as the present HE-BMG, in which the annealed glassy ribbon sample was obtained by annealing the as-quenched glassy ribbon at 793 K for 5 min in a vacuum quartz tube. The coercivity (H_c) was measured with a B-H loop tracer (EXPH-100) under the maximum applied field of 800 A/m. The permeability (μ_e) at the frequency of 1 kHz is measured by an impedance analyzer under a field of 1 A/m. The hysteresis loss (P) at the frequency of 50 Hz was measured by AC B-H loop tracer with a maximum applied field of 0.9 T. The magnetic domains on the air-bare surface of the as-quenched glassy ribbon samples were observed by Kerr microscopy under the field of 1 mT, without further sample preparation such as polishing or coating. The mechanical properties under compressive load were measured using an Instron mechanical testing machine (Reger, RGM-4100) with the strain rate of $1 \times 10^{-4}\,s^{-1}$ at room temperature. The gauge dimension of the samples for compressive test was 1 mm in diameter and 2 mm in height. At least five samples were measured to ensure the reproducibility of the data in the compression test. The fracture surface of the compressive samples was observed with a scanning electron microscope (SEM, Zeiss Supra 55). All the measurements were performed at room temperature.

3. Results and discussion

Fig. 1(a) shows the DSC thermal scan at a heating rate of 0.33 K/s and XRD patter of the as-prepared $(Fe_{1/3}Co_{1/3}Ni_{1/3})_{80}(P_{1/2}B_{1/2})_{20}$ alloy rod with a diameter of 2 mm. It can be seen that the sample shows a clear glass transition, followed by an extended supercooled liquid region and a single-stage of crystallization process. The glass transition temperature (T_g) and the onset crystallization temperature (T_x) of the sample can be determined from the DSC curve to be 686 K and 712 K, respectively. The XRD pattern of the sample (inset in Fig. 1(a)) reveals a typical broad diffraction maximum without any distinct crystalline peaks, indicating a fully glassy structure. The bright field image of the sample shows a homogeneous background and the corresponding selected area electron diffraction (SAED) pattern consist of halos as shown in Fig. 1(b). And the HRTEM image of the sample show typical amorphous characteristics and fully random arrangement of atoms as shown in Fig. 1(c). These further confirm that the sample has the homogeneous glassy structure.

The present $(Fe_{1/3}Co_{1/3}Ni_{1/3})_{80}(P_{1/2}B_{1/2})_{20}$ HE-BMG exhibits better glass forming ability (GFA) with a critical diameter of 2 mm compared with other transition metal based HE-BMGs (see Table 1). The HEAs can form a simple fcc/bcc/hcp solid solution structure or a BMG. The phase evolution in HEAs can be controlled

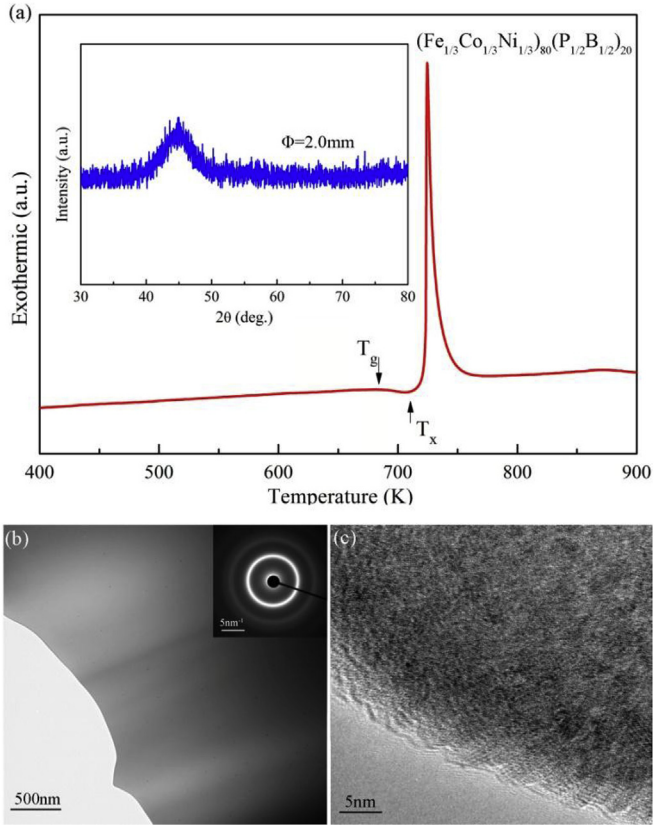

Fig. 1. DSC curve and XRD pattern (inset) (a), the bright field image and the corresponding SAED patterns (inset) (b), and HRTEM image of the as-prepared $(Fe_{1/3}Co_{1/3}Ni_{1/3})_{80}(P_{1/2}B_{1/2})_{20}$ HE-BMG (c).

Table 1
Glass transition temperature (T_g), supercooled liquid region (ΔT_x), critical diameter for glass formation (d_c), fracture strength (σ_f), plastic strain (ε_p), saturation magnetization (J_s) of the present $(Fe_{1/3}Co_{1/3}Ni_{1/3})_{80}(P_{1/2}B_{1/2})_{20}$ high entropy bulk metallic glass together with some selected high entropy bulk metallic glasses.

Composition (at.%)	T_g (K)	ΔT_x (K)	d_c (mm)	σ_f (MPa)	ε_p (%)	J_s (T)
$Ti_{20}Zr_{20}Hf_{20}Cu_{20}Ni_{20}$ [9]	658	53	1.5	1920	0.3	–
$Sr_{20}Ca_{20}Yb_{20}Mg_{20}Zn_{20}$ [39]	353	37	1	382	0	–
$Fe_{25}Co_{25}Ni_{25}(B_{0.6}Si_{0.4})_{25}$ [16]	771	37	1	3239	3.1	0.84
$Fe_{25}Co_{25}Ni_{25}(B_{0.7}Si_{0.3})_{25}$ [16]	767	40	1.5	3624	1.7	0.87
$Fe_{25}Co_{25}Ni_{25}(P_{0.5}C_{0.3}B_{0.2})_{25}$ [15]	674	56	1	2850	1.2	0.86
$Fe_{25}Co_{25}Ni_{25}(P_{0.3}C_{0.3}B_{0.4})_{25}$ [15]	702	47	1	3210	0.3	0.8
$Fe_{25}Co_{25}Ni_{25}(P_{0.5}C_{0.1}B_{0.2}Si_{0.2})_{25}$ [10]	707	39	2	3076	1.9	0.8
$Fe_{25}Co_{25}Ni_{25}(P_{0.4}C_{0.1}B_{0.3}Si_{0.2})_{25}$ [10]	720	39	1.5	–	–	0.83
$(Fe_{1/3}Co_{1/3}Ni_{1/3})_{80}(P_{1/2}B_{1/2})_{20}$ (This work)	686	26	2	3000	4	0.90

by a topology natured atomic size polydispersity (δ), chemistry natured mixing enthalpy (ΔH_{mix}) and mixing entropy (ΔS_{mix}), which are defined as the following equations:

$$\delta = 100\sqrt{\sum_{i-1}^{N} c_i(1 - r_i/\bar{r})^2} \quad (1)$$

$$\Delta H_{mix} = \sum_{i\neq 1, i\neq j}^{N} \Omega_{ij} c_i c_j \quad (2)$$

$$\Delta S_{mix} = -R\sum_{i=1}^{N} c_i \ln c_i \quad (3)$$

where N is the number of the components in an alloy system; c_i is the atomic fraction of the i-th component; $\bar{r}$ is the average atomic radius; r_i is the atomic radius of the i-th component, which can be obtained in Reference [19]; Ω_{ij} ($=4\Delta H_{AB}^{mix}$) is the interaction parameter from regular solution model between the i-th and j-th elements, and ΔH_{AB}^{mix} is the mixing enthalpy of binary liquid alloys [20]; R is the gas constant. It is pointed out that HEA-BMG can form when the δ, ΔH_{mix} and ΔS_{mix} simultaneously satisfy $\delta \geq 9$, $-49 \leq \Delta H_{mix} \leq 5.5$ kJ/mol, and $7 \leq \Delta S_{mix} \leq 16$ J/(K.mol) [21,22]. For the present HE-BMG system, the atomic radii of Fe, Co, Ni, B, and P elements are 0.1241, 0.1251, 0.1246, 0.0820, and 0.130 nm, respectively [19], and the values of ΔH_{mix} between atomic pairs are lists in Table 2 [20]. Accordingly, the δ, ΔH_{mix} and ΔS_{mix} parameters for the $(Fe_{1/3}Co_{1/3}Ni_{1/3})_{80}(P_{1/2}B_{1/2})_{20}$ alloy are calculated to be 11.15, −20.41 kJ/mol and 12.61 J/(K.mol), respectively, which are located within the proposed glass formation range. A large δ, negative ΔH_{mix} and high ΔS_{mix} are three important factors in the formation of amorphous phase. A large δ due to the formation of amorphous phase shall originate from the requirement on the sufficient atomic-level stress to destabilize the solid solution phase [23,24]. Further, a large δ and negative ΔH_{mix} will improve the local packing efficiency and restrain the long-range diffusion of atoms. Consequently, the crystalline phase formation will be suppressed during the cooling process, thus leading to a high GFA [25,26]. In addition, high ΔS_{mix} could enhance the confusion level, complicate competing crystalline phases and frustrate the process of crystallization, which is benefit for the formation of amorphous phase [27]. As mentioned above, the present $Fe_{26.7}Co_{26.7}Ni_{26.7}B_{10}P_{10}$ HE-BMGs simultaneously possess large δ, ΔH_{mix} and ΔS_{mix}, and therefore obtain a large GFA.

Table 2
Mixing enthalpies between Fe, Co, Ni, P and B atoms.

ΔH_{mix} (kJ/mol)	Fe	Co	Ni	B	P
Fe	–	−1	−2	−26	−39.5
Co	−1	–	0	−24	−35.5
Ni	−2	0	–	−24	−34.5
B	−26	−24	−24	–	0.5
P	−39.5	−35.5	−34.5	0.5	–

Fig. 2(a) presents hysteresis loop of the as-prepared $(Fe_{1/3}Co_{1/3}Ni_{1/3})_{80}(P_{1/2}B_{1/2})_{20}$ HE-BMG sample at room temperature. The sample exhibits a saturation magnetization (J_s) of 0.90 T, which is the highest one reported to date for transition metal based HE-

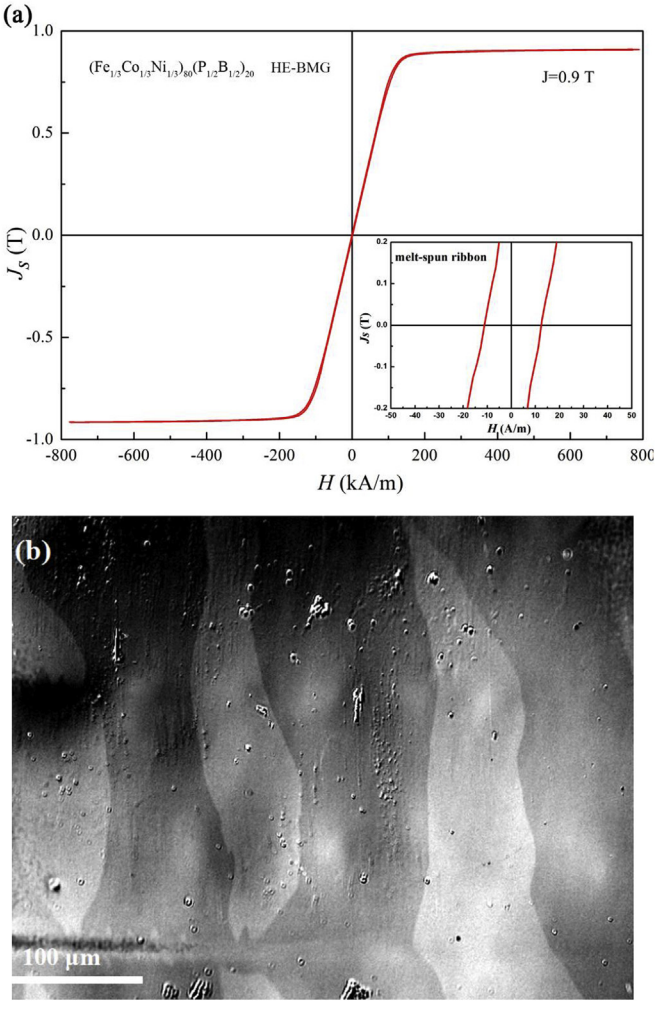

Fig. 2. (a) Hysteresis loop of the as-prepared $(Fe_{1/3}Co_{1/3}Ni_{1/3})_{80}(P_{1/2}B_{1/2})_{20}$ HE-BMG and enlarged B-H loops of the as-quenched melt-spun ribbon (inset); (b) Magnetic domains of the as-quenched melt-spun ribbon obtained by Magneto-optical Kerr microscopy under the field of 1 mT.

BMGs. The high saturation magnetization should be attributed to high magnetic elements content in the present $(Fe_{1/3}Co_{1/3}Ni_{1/3})_{80}(P_{1/2}B_{1/2})_{20}$ HE-BMG. The coercivity, permeability @ 1 kHz and hysteresis loss @ 50 Hz are determined to be 12 A/m, 1580 and 113 kJ/mol, respectively, for the as-quenched $(Fe_{1/3}Co_{1/3}Ni_{1/3})_{80}(P_{1/2}B_{1/2})_{20}$ glassy ribbon, and 1.5 A/m, 10174 and 21 kJ/mol, respectively, for the $(Fe_{1/3}Co_{1/3}Ni_{1/3})_{80}(P_{1/2}B_{1/2})_{20}$ glassy ribbon annealed at 793 K for 5 min, indicating excellent soft magnetic properties of the present HE-BMG. The low coercivity of the present HE-BMG should be attributed to its glassy structure including lack of defects and other large-scale structural inhomogeneities, which leads to greater mobility of magnetic domain walls. For further understanding the good soft magnetic properties of the present $(Fe_{1/3}Co_{1/3}Ni_{1/3})_{80}(P_{1/2}B_{1/2})_{20}$ HE-BMG, magnetic domains of the as-quenched amorphous ribbon sample with the same composition are observed with Magneto-optical Kerr Microscopy. As shown in Fig. 2 (b), the ribbon exhibits stripe domains which are almost parallel to the ribbon direction. In addition, the domains in as-quenched ribbon sample are relatively smooth and wide. It is well accepted that the domain wall energy $\gamma_B \propto D_0^{-2}$, where D_0 corresponds to domain width [28]. The widen of domain should be attributed to the lower domain wall energy γ_B, which is correlated to the pinning effects induced by internal stress and/or anisotropy fluctuations of the materials [29].

Fig. 3(a) shows the room temperature compressive stress-strain curve of the as-prepared $(Fe_{1/3}Co_{1/3}Ni_{1/3})_{80}(P_{1/2}B_{1/2})_{20}$ HE-BMG. It can be found that the sample has a linearly elastic response followed by an apparently yielding behavior at about 3000 MPa. Moreover, there is a distinct plastic flow (ε_p) of about 4%. To the best of our knowledge, the plastic strain is the largest among the reported transition metal based HE-BMGs until now (see Table 1). Fig. 3(b) and (c) show the SEM images of the lateral and fracture surface morphologies of the failure sample, respectively.

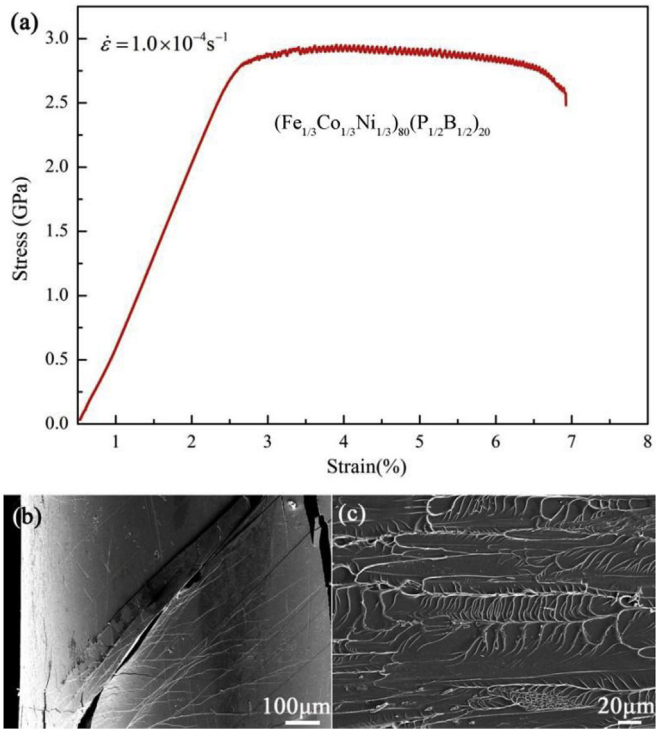

Fig. 3. Room temperature compressive stress-strain curve (a) of as-prepared $(Fe_{1/3}Co_{1/3}Ni_{1/3})_{80}(P_{1/2}B_{1/2})_{20}$ HE-BMG rod, and SEM images of lateral (b) and fracture surface (c) morphologies of the failure sample.

Accordingly, multiple shear bands can be found on the lateral surface. More importantly, there are many secondary shear bands that distribute widely among the primary shear bands. It is accepted that BMG can be regarded as a material consisting of elastic matrix and liquid-like regions with high density of free volume [30,31]. Upon loading, the liquid-like regions will act as the potential sites of shear transformation zones (STZs), which are the unit carriers of plasticity in BMG [32,33]. As the external stress keeps increasing, primary shear band will nucleate due to the activation of stress-assisted STZs [34,35]. Subsequently, the primary shear band will either propagate continuously until catastrophic fracture or arrested by the elastic matrix and followed by the nucleation of new shear band. The former corresponds to the poor plasticity, while the latter means the large plastic strain. The underlying mechanism could be ascribed to the energy dissipation competition between the nucleation of new shear bands and propagation of the primary shear bands [36]. If the energy dissipated for nucleation overtakes that needed for shear band growth, shear band propagation would be easier to take place than nucleation. If the nucleation of shear band needs less energy than propagation, shear band nucleation would be more active than propagation. In the present work, the heat fluctuation resulted from the propagation of primary shear band could be neglected [37]. Additionally, the associated atomic rearrangements triggered by the formation of primary shear band could relax the local stress and make the material in the primary shear band denser than the liquid-like regions around it. In this case, shear band nucleation will need less energy than its propagation. Consequently, the primary shear band would be arrested and secondary or other shear band would be formed. This is consistent with the multiple shear bands on the lateral surface of the deformed sample presented in Fig. 3(b). From Fig. 3(c), vein-like patterns can be observed on the fracture surface, which demonstrates the typical compressive shear fracture and the good toughness of the present HE-BMG [33,38].

4. Conclusion

The $(Fe_{1/3}Co_{1/3}Ni_{1/3})_{80}(P_{1/2}B_{1/2})_{20}$ HE-BMG with the maximum diameter of 2 mm has been prepared by combining fluxing treatment and J-quenching technique. The present HE-BMG exhibits a high saturation magnetization of 0.90 T, low coercivity of 1.5 A/m, high permeability of 10174 @ 1 kHz, low hysteresis loss of 21 kJ/mol @ 50 Hz, high fracture strength of 3000 MPa and distinct plastic strain of 4%. Compared with the reported transition metal based HE-BMGs, the present newly developed HE-BMG possesses better GFA, superior soft magnetic and mechanical properties, and thus shows a future promising application as advanced structural and functional materials.

Acknowledgements

This research was sponsored by National Natural Science Foundation of China (Grant No. 51561028 and 51771161).

References

[1] M.M. Trexler, N.N. Thadhani, Mechanical properties of bulk metallic glasses, Prog. Mater. Sci. 55 (2010) 759–839.
[2] T.C. Hufnagel, C.A. Schuh, M.L. Falk, Deformation of metallic glasses: recent developments in theory, simulations, and experiment, Acta Mater. 109 (2016) 375–393.
[3] Y. Zhang, T.T. Zuo, Z. Tang, M.C. Gao, K.A. Dahmen, P.K. Liaw, Z.P. Lu, Microstructures and properties of high-entropy alloys, Prog. Mater. Sci. 61 (2014) 1–93.
[4] B. Cantor, I.T.H. Chang, P. Knight, A.J.B. Vincent, Microstructural development in equiatomic multicomponent alloys, Mater. Sci. Eng. A 375–377 (2004) 213–218.

[5] Y.J. Zhao, J.W. Qiao, S.G. Ma, M.C. Gao, H.J. Yang, M.W. Chen, Y. Zhang, A hexagonal close-packed high-entropy alloy: the effect of entropy, Mater. Des. 96 (2016) 10–15.
[6] J.Y. He, H. Wang, H.L. Huang, X.D. Xu, M.W. Chen, Y. Wu, X.J. Liu, T.G. Nieh, K. An, Z.P. Lu, A precipitation-hardened high-entropy alloy with outstanding tensile properties, Acta Mater. 102 (2016) 187–196.
[7] Z. Li, K.G. Pradeep, Y. Deng, D. Raabe, C.C. Tasan, Metastable high-entropy dual-phase alloys overcome the strength–ductility trade-off, Nature 534 (2016) 227.
[8] B. Gludovatz, A. Hohenwarter, D. Catoor, E.H. Chang, E.P. George, R.O. Ritchie, A fracture-resistant high-entropy alloy for cryogenic applications, Science 345 (2014) 1153.
[9] L. Ma, L. Wang, T. Zhang, A. Inoue, Bulk glass formation of Ti-Zr-Hf-Cu-M (M=Fe, Co, Ni) alloys, Mater. Trans. 43 (2002) 277–280.
[10] Y. Xu, Y. Li, Z. Zhu, W. Zhang, Formation and properties of $Fe_{25}Co_{25}Ni_{25}(P, C, B, Si)_{25}$ high-entropy bulk metallic glasses, J. Non-Cryst. Solids 487 (2018) 60–64.
[11] R. Wei, J. Tao, H. Sun, C. Chen, G.W. Sun, F.S. Li, Soft magnetic $Fe_{26.7}Co_{26.7-}Ni_{2.6.6}Si_9B_{11}$ high entropy metallic glass with good bending ductility, Mater. Lett. 97 (2017) 87–89.
[12] A. Takeuchi, N. Chen, T. Wada, Y. Yokoyama, H. Kato, A. Inoue, J.W. Yeh, $Pd_{20}Pt_{20}Cu_{20}Ni_{20}P_{20}$ high-entropy alloy as a bulk metallic glass in the centimeter, Intermetallics 19 (2011) 1546–1554.
[13] J. Li, L. Xue, W. Yang, C. Yuan, J. Huo, B. Shen, Distinct spin glass behavior and excellent magnetocaloric effect in $Er_{20}Dy_{20}Co_{20}Al_{20}RE_{20}$ (RE = Gd, Tb and Tm) high-entropy bulk metallic glasses, Intermetallics 96 (2018) 90–93.
[14] S.F. Zhao, G.N. Yang, H.Y. Ding, K.F. Yao, A quinary Ti–Zr–Hf–Be–Cu high entropy bulk metallic glass with a critical size of 12 mm, Intermetallics 61 (2015) 47–50.
[15] Y. Li, W. Zhang, T. Qi, New soft magnetic $Fe_{25}Co_{25}Ni_{25}(P, C, B)_{25}$ high entropy bulk metallic glasses with large supercooled liquid region, J. Alloys Compd. 693 (2017) 25–31.
[16] T. Qi, Y. Li, A. Takeuchi, G. Xie, H. Miao, W. Zhang, Soft magnetic $Fe_{25}Co_{25-}Ni_{25}(B, Si)_{25}$ high entropy bulk metallic glasses, Intermetallics 66 (2015) 8–12.
[17] C. Suryanarayana, A. Inoue, Iron-based bulk metallic glasses, Int. Mater. Rev. 58 (2013) 131–166.
[18] Q. Li, J. Li, P. Gong, K. Yao, J. Gao, H. Li, Formation of bulk magnetic ternary $Fe_{80}P_{13}C_7$ glassy alloy, Intermetallics 26 (2012) 62–65.
[19] S. Guo, C.T. Liu, Phase stability in high entropy alloys: formation of solid-solution phase or amorphous phase, Prog. Nat. Sci. Mater. Int. 21 (2011) 433–446.
[20] A. Takeuchi, A. Inoue, Classification of bulk metallic glasses by atomic size difference, heat of mixing and period of constituent elements and its application to characterization of the Main alloying element, Mater. Trans. 46 (2005) 2817–2829.
[21] Y. Zhang, Y.J. Zhou, J.P. Lin, G.L. Chen, P.K. Liaw, Solid-solution phase formation rules for Multi-component alloys, Adv. Eng. Mater. 10 (2008) 534–538.
[22] S. Guo, C.T. Liu, Phase stability in high entropy alloys: formation of solid-solution phase or amorphous phase, Prog. Mater. Sci. 21 (2011) 433–446.
[23] T. Egami, Y. Waseda, Atomic size effect on the formability of metallic glasses, J. Non-Cryst. Solids 6 (1984) 113–134.
[24] T. Egami, V. Levashov, R. Aga, J.R. Morris, Geometrical frustration and glass formation, Metall. Mater. Trans. A 39 (2008) 1786.
[25] A. Inoue, T. Zhang, N. Nishiyama, K. Ohba, T. Masumoto, Preparation of 16 mm diameter rod of amorphous $Zr_{65}Al_{7.5}Ni_{10}Cu_{17.5}$ alloy, Mater. Trans., JIM 34 (1993) 1234–1237.
[26] X.H. Lin, W.L. Johnson, Formation of Ti–Zr–Cu–Ni bulk metallic glasses, J. Appl. Phys. 78 (1995) 6514–6519.
[27] A.L. Greer, Confusion by design, Nature 366 (1993) 303–304.
[28] H. Kronmuller, M. Fahnle, M. Domann, H. Grimm, R. Grimm, B. Groger, Magnetic properties of amorphous ferromagnetic alloys, J. Magn. Magn. Mater. 13 (1979) 53–70.
[29] T. Bitoh, A. Makino, A. Inoue, Origin of low coercivity of Fe-(Al, Ga)-(P, C, B, Si, Ge) bulk glassy alloys, Mater. Trans. 44 (2003) 2020–2024.
[30] J.C. Ye, J. Lu, C.T. Liu, Q. Wang, Y. Yang, Atomistic free-volume zones and inelastic deformation of metallic glasses, Nat. Mater. 9 (2010) 619–623.
[31] Z. Lu, X.N. Yang, B.A. Sun, Y.Z. Li, K. Chen, W.H. Wang, H.Y. Bai, Divergent strain acceleration effects in metallic glasses, Scripta Mater. 130 (2017) 229–233.
[32] C. Wang, Q.P. Cao, X.D. Wang, D.X. Zhang, U. Ramamurty, R.L. Narayan, J. Jiang, Intermediate temperature brittleness in metallic glasses, Adv. Mater. 29 (2017) 1605537–1605542.
[33] M.C. Li, M.Q. Jiang, S. Yang, F. Jiang, L. He, J. Sun, Effect of strain rate on yielding strength of a Zr-based bulk metallic glass, Mater. Sci. Eng. A 680 (2017) 21–26.
[34] E.R. Homer, C.A. Schuh, Mesoscale modeling of amorphous metals by shear transformation zone dynamics, Acta Mater. 57 (2009) 2823–2833.
[35] A.L. Greer, Y.Q. Cheng, E. Ma, Shear bands in metallic glasses, Mater. Sci. Eng. R 74 (2013) 71–132.
[36] Y. Chen, M.Q. Jiang, L.H. Dai, Collective evolution dynamics of multiple shear bands in bulk metallic glasses, Int. J. Plast. 50 (2013) 18–36.
[37] Y.Q. Cheng, Z. Han, Y. Li, E. Ma, Cold versus hot shear banding in bulk metallic glass, Phys. Rev. B 80 (2009) 134115.
[38] J. Zhou, W. Yang, C. Yuan, B. Sun, B. Shen, Ductile FeNi-based bulk metallic glasses with high strength and excellent soft magnetic properties, J. Alloys Compd. 742 (2018) 318–324.
[39] K. Zhao, W. Jiao, J. Ma, X.Q. Gao, W.H. Wang, Formation and properties of Sr-based bulk metallic glasses with ultralow glass transition temperature, J. Mater. Res. 27 (2012) 2593–2600.